Searching for charged Higgs bosons via $e^+e^- \to H^\pm W^\mp S$ at the ILC

Brahim Ait Ouazghour,[1,*] Abdesslam Arhrib,[2,3,†] Kingman Cheung,[3,4,‡] Es-said Ghourmin,[5,§] Mohamed Krab,[6,∥] and Larbi Rahili[5,¶]

[1]*LPHEA, Physics Department, FSSM, Cadi Ayyad University, P.O.B. 2390 Marrakech, Morocco*
[2]*Abdelmalek Essaadi University, Faculty of Sciences and Techniques, Tanger, Morocco*
[3]*Department of Physics and CTC, National Tsing Hua University, Hsinchu, Taiwan 300*
[4]*Division of Quantum Phases and Devices, School of Physics, Konkuk University, Seoul 143-701, Republic of Korea*
[5]*Laboratory of Theoretical and High Energy Physics (LPTHE), Faculty of Science, Ibnou Zohr University, B.P 8106, Agadir, Morocco*
[6]*Department of Physics, National Taiwan University, Taipei 10617, Taiwan*

(Received 5 June 2025; accepted 28 August 2025; published 16 September 2025)

We investigate the phenomenology of the charged Higgs boson at the International Linear Collider (ILC) within the framework of the type-X Two-Higgs Doublet Model, where a light charged Higgs boson, with a mass around 200 GeV or even smaller than top quark mass, is still being consistent with flavor physics data as well as with collider experimental data. In the theoretically and experimentally allowed parameter space, the $e^+e^- \to H^\pm W^\mp S$ (with $S = H, A$) production processes can yield signatures with event rates larger than those from $e^+e^- \to H^+H^-$ and offer sensitivity to the Higgs mixing parameter $\sin(\beta - \alpha)$. We consider the bosonic $H^\pm \to W^\pm S$ decays, where the neutral scalar S further decays into a pair of tau leptons. We show, through a detector-level Monte Carlo analysis, that the resulting $[\tau\tau][\tau\tau]WW$ final state could be seen at the ILC with at least 500 GeV center-of-mass energy and 500 fb^{-1} of luminosity.

DOI: 10.1103/rf5m-wb6y

I. INTRODUCTION

The discovery of the Standard Model (SM) Higgs boson by ATLAS [1] and CMS [2] experiments has completed the particle spectrum defined by the SM. However, many questions remain unanswered. These include theoretical challenges, such as the mechanism that stabilizes the electroweak scale and the generation of neutrino masses, as well as empirical issues like the nature of dark matter and the matter-antimatter asymmetry. As a result, there is a strong motivation to investigate theories beyond the SM (BSM) that operate near the TeV scale [3–7]. Many BSM theories naturally feature an extended Higgs sector. A prominent example of this is the two Higgs doublet model (2HDM), which adds an additional electroweak Higgs doublet, enriching the theory with a variety of new Higgs boson phenomena and implications for flavor physics. Intense searches for these novel Higgs bosons have been conducted at colliders, particularly at the LHC, which has played a significant role in these efforts (for a comprehensive overview, see Ref. [8] and the references therein). The lack of observed signals has resulted in current limits on the mass and couplings of these non-SM Higgs bosons. The High Luminosity LHC (HL-LHC) is expected to enhance several earlier measurements and may provide evidence for new physics. However, to advance the precise Higgs measurement program initiated at the LHC, it is essential to establish a controlled environment, such as an electron-positron Higgs factory. This would facilitate a thorough investigation of the properties of the recently discovered Higgs boson, similar to those in the SM, and could even enable the discovery of new particles. Several projects involving e^+e^- machines are currently in the planning stages, including initiatives like the Circular Electron Positron Collider [9], the Compact Linear Collider (CLIC) [10,11], the Future Circular Collider [12,13], and the International Linear Collider (ILC) [14,15].

These projects aim to provide an ideal setting for intricate investigations into the properties of the Higgs

*Contact author: b.ouazghour@gmail.com
†Contact author: aarhrib@gmail.com
‡Contact author: cheung@phys.nthu.edu.tw
§Contact author: s.ghourmin123@gmail.com
∥Contact author: mkrab@hep1.phys.ntu.edu.tw
¶Contact author: rahililarbi@gmail.com

boson and potentially discover new particles. Recent investigations have indeed highlighted the remarkable prospects these colliders present in exploring the electroweak sector. This includes endeavors such as precise measurements of Higgs boson couplings [16], the detection of electroweak dark matter [17,18], study of neutrinos [19,20], and the potential discovery of other BSM particles [21–23].

Existence of charged Higgs bosons is a generic prediction of multiple extensions of the SM Higgs sector, such as the 2HDM. The charged Higgs bosons can be produced and explored at the LHC. We refer to Ref. [24] for an extensive review on charged Higgs phenomenology at the LHC. A light $H^\pm$ can be copiously produced from $t\bar{t}$ production followed by $t \to bH^+$ if kinematically allowed (i.e., $m_{H^\pm} < m_t - m_b$). When its exceeds the top quark mass, the processes $gb \to tH^-$ and $gg \to \bar{t}bH^+$ [25] are typically used for $H^\pm$ searches.

Charged Higgs production can proceed at the ILC [26,27] or CLIC [10] through $e^+e^- \to \gamma^*, Z^* \to H^+H^-$ or $e^+e^- \to \tau^\pm\nu_\tau H^\mp$ and $e^+e^- \to t\bar{b}H^-$ [28–31] and the loop mediated process $e^+e^- \to W^\pm H^\mp$ [32,33]. At high energy, one can also have vector boson fusion: $e^+e^- \to \nu\bar{\nu}H^+H^-$ [34]. The production of a charged Higgs boson at muon colliders is rather similar to e^+e^-; it can proceed through several processes. Production processes $\mu^+\mu^- \to H^+H^-$, $\mu^+\mu^- \to H^\pm W^\mp$, and $\mu^+\mu^- \to \nu\bar{\nu}H^+H^-$ have been studied in Ref. [34].

Charged Higgs bosons have been searched for at LEP [35] through $e^+e^- \to H^+H^-$, followed by the fermionic $H^\pm \to \tau\nu$ and $H^\pm \to cs$ decays, where a limit of $m_{H^\pm} \geq 80$ GeV was obtained assuming $H^\pm \to W^\pm A$ is absent. If the latter is present, a limit of $m_{H^\pm} \geq 72.5$ GeV (2HDM type-I) was obtained [36] assuming $m_A = 12$ GeV. At the Tevatron, charged Higgs bosons have also been searched for in top quark decays with subsequent $\tau\nu$ or cs decays [37,38]. These searches set upper limits on $\mathrm{BR}(t \to bH^\pm)$ for different $H^\pm$ decay scenarios. At the LHC, charged Higgs bosons have been searched for in $H^\pm \to \tau\nu$ [39–50], cs [51–54], cb[1] [55,57], and tb [47,58–62] decays. All the aforementioned searches are conventional without considering bosonic decays. However, if bosonic decay channels $H^\pm \to W^{\pm(*)}S$ ($S = h, H, A$) are kinematically accessible, they can offer distinctive signatures and could be promising avenues for discovery [63–70]. A few experimental efforts have begun probing these channels [71–74], but they remain limited. See, e.g., Ref. [75] for a recent detailed study of collider search limits on charged Higgs bosons in the four types of the 2HDM. See also Ref. [76] for a discussion of charged Higgs boson searches at the LHC and their prospects at the high-luminosity LHC.

In this study, we investigate the production of charged Higgs bosons in association with a W boson and a non-SM Higgs boson, i.e., $e^+e^- \to H^\pm W^\mp S$, where $S = H$ or A, within the framework of the type-X 2HDM. Our numerical results are provided after thoroughly exploring the 2HDM parameter space, adhering to various theoretical (perturbative unitarity, perturbativity, and vacuum stability) and experimental [derived from SM-like Higgs boson discovery data, BSM Higgs bosons exclusion data, electroweak precision tests, and flavor physics] constraints. We perform a comprehensive Monte Carlo analysis and gauge the sensitivity at center-of-mass energies of 500, 1000, and 1500 GeV of the ILC.

II. 2HDM

In the 2HDM, in addition to the SM scalar doublet Φ_1, an additional doublet Φ_2 with hypercharge $+1$ is added to the Higgs sector, assuming that charge-parity (CP) is not spontaneously broken. The two Higgs scalar doublets can be parametrized as

$$\Phi_1 = \begin{pmatrix} \phi_1^+ \\ \phi_1^0 \end{pmatrix} \quad \text{and} \quad \Phi_2 = \begin{pmatrix} \phi_2^+ \\ \phi_2^0 \end{pmatrix}, \tag{1}$$

with $\phi_1^0 = (v_1 + \psi_1 + i\eta_1)/\sqrt{2}$, $\phi_2^0 = (v_2 + \psi_2 + i\eta_2)/\sqrt{2}$, and $\sqrt{v_1^2 + v_2^2} = v = 246$ GeV. The general scalar potential invariant under the electroweak gauge group $SU(2)_L \times U(1)_Y$ can be expressed as [77]

$$\begin{aligned} V(\Phi_1,\Phi_2) &= m_{11}^2\Phi_1^\dagger\Phi_1 + m_{22}^2\Phi_2^\dagger\Phi_2 - [m_{12}^2\Phi_1^\dagger\Phi_2 + \mathrm{H.c.}] \\ &\quad + \frac{\lambda_1}{2}(\Phi_1^\dagger\Phi_1)^2 + \frac{\lambda_2}{2}(\Phi_2^\dagger\Phi_2)^2 \\ &\quad + \lambda_3(\Phi_1^\dagger\Phi_1)(\Phi_2^\dagger\Phi_2) + \lambda_4(\Phi_1^\dagger\Phi_2)(\Phi_2^\dagger\Phi_1) \\ &\quad + \left\{\frac{\lambda_5}{2}(\Phi_1^\dagger\Phi_2)^2 + \mathrm{H.c.}\right\}, \end{aligned} \tag{2}$$

where m_{11}^2, m_{22}^2, and m_{12}^2 parameters as well as the λ_i ($i = 1, 2, 3, 4, 5$) couplings are assumed to be real to ensure that the potential is CP conserving. A discrete Z_2 symmetry is also assumed in order to avoid flavor changing neutral currents (FCNCs) at the tree level. Such a Z_2 symmetry is softly broken by the bilinear term proportional to m_{12}^2 parameter.

After electroweak symmetry breaking, the 8 degrees of freedom initially present in the two Higgs doublet fields are reduced. Three of these degrees of freedom are absorbed by the Goldstone bosons, giving mass to the gauge bosons $W^\pm$ and Z. We are then left with five physical Higgs states: a pair of charged Higgs $H^\pm$, a CP-odd state A, and two CP-even states (H and h with $m_h < m_H$). One of the

[1]ATLAS reported a charged Higgs excess at $m_{H^\pm} = 130$ GeV [55]; see, e.g., Ref. [56] for a possible interpretation within 2HDM type-III.

TABLE I. Yukawa couplings of the h, H, and A Higgs bosons to fermions in 2HDM type X.

Model	κ_h^u	κ_h^d	κ_h^l	κ_H^u	κ_H^d	κ_H^l	κ_A^u	κ_A^d	κ_A^l
Type X	c_α/s_β	c_α/s_β	$-s_\alpha/c_\beta$	s_α/s_β	s_α/s_β	c_α/c_β	c_β/s_β	$-c_\beta/s_\beta$	$\tan\beta$

neutral CP-even Higgs can be identified as the 125 GeV Higgs-like particle observed at the LHC. The combination $v^2 = v_1^2 + v_2^2 = (2\sqrt{2}G_F)^{-1}$ can be used to fix one of the vacuum expectation values as a function of the Fermi constant G_F and $\tan\beta$. Together with the two minimization conditions, the model has seven independent parameters,

$$\alpha, \tan\beta(= v_2/v_1), \quad m_h, \quad m_H, \quad m_A, \quad m_{H^\pm}, \quad \text{and} \quad m_{12}^2, \tag{3}$$

where α and β are, respectively, the CP-even and CP-odd mixing angles. Here, we assume that h is the observed SM-like Higgs boson at the LHC with $m_h = 125.09$ GeV; therefore, we are left with only six free parameters.

In the Yukawa sector, if we assume that both Higgs doublets couple to all fermions, like in the SM, we will end up with a large tree-level FCNCs mediated by the neutral Higgs scalars. To prevent such large FCNCs at the tree level, the 2HDM needs to satisfy Paschos-Glashow-Weinberg theorem [78,79], which asserts that all fermions with the same quantum numbers couple to the same Higgs multiplet. One can have four different types of Yukawa textures depending on how the doublets Φ_1 and Φ_2 interact with the fermions. In the 2HDM type I, only the second doublet Φ_2 interacts with all the fermions. In type II, Φ_2 interacts with up-type quarks, and Φ_1 interacts with the charged leptons and down-type quarks, while in type-Y (or flipped) down-type quarks couple to Φ_1, while charged leptons and up-type quarks couple to Φ_2. In type X, Φ_2 couples to quarks, and Φ_1 couples to leptons.

In terms of the mass eigenstates of the neutral and charged Higgs bosons, the Yukawa interactions can be written as

$$\begin{aligned} -\mathcal{L}_Y = &\sum_{f=u,d,\ell} \frac{m_f}{v}[\kappa_h^f \bar{f} f h + \kappa_H^f \bar{f} f H - i\kappa_A^f \bar{f}\gamma_5 f A] \\ &+ \frac{\sqrt{2}}{v}[\bar{u}_i V_{ij}(m_{u_i}\kappa_A^u P_L + \kappa_A^d m_{d_j} P_R) d_j H^+] \\ &+ \frac{\sqrt{2}}{v}\bar{\nu}_L \kappa_A^\ell m_\ell \ell_R H^+ + \text{H.c.}, \end{aligned} \tag{4}$$

where κ_S^f ($S = h, H, A$) are the Yukawa couplings listed in Table I for the type-X 2HDM and V_{ij} are Cabibbo-Kobayashi-Maskawa (CKM) matrix elements. In what follows, we use the notation of $s_x = \sin x$ and $c_x = \cos x$.

The reduced coupling of the lighter Higgs boson, h, to either WW or ZZ is given by $s_{\beta-\alpha}$; on the other hand, the coupling of the heavier Higgs boson, H, is equivalent to the SM coupling multiplied by $c_{\beta-\alpha}$. Notably, the coupling between the pseudoscalar, A, and vector bosons is absent due to CP symmetry invariance.

III. NUMERICAL ANALYSIS

We perform a general scan over the 2HDM parameter space, as given in Table II, to explore scenarios that may result in a significant cross section for our processes $e^+e^- \to H^\pm W^\mp S$ ($S = H$, A). We use the code 2HDMC-1.8.0 [80] to numerically scan the parameter space, check theoretical constraints, and compute the S, T, and U oblique parameters. Our parameter points are further checked for consistency with experimental constraints from the direct searches for additional Higgs bosons and agreement with the Higgs signal measurements using the public codes HiggsBounds [81] and HiggsSignals [82]. Additionally, B-physics constraints are checked using SuperIso [83].

After scrutinizing the parameter space of the model with the theoretical and experimental constraints, the resulting parameter points are passed to FormCalc [84–86] to compute the corresponding cross section of each process at the e^+e^- collider.

Meanwhile, the charged Higgs boson can be produced associated with the $W^\pm$ boson and the neutral Higgs boson via the processes $e^+e^- \to \{H^\pm W^\mp H, H^\pm W^\mp A\}$. The relevant Feynman diagrams are shown in Fig. 1. Most of the Feynman diagrams are mediated by the s-channel photon or Z exchange, with the exception of the last one, d_6, which requires t-channel mediation by neutrino exchange. The couplings involved in $e^+e^- \to H^\pm W^\mp H/A$ are pure gauge couplings, and in this regard, the cross section of the process is not strongly sensitive to the Yukawa textures.

TABLE II. 2HDM type-X input parameters.

Parameters	Scan range
m_h	125.09 GeV
m_H	[130, 1000] GeV
$m_{A,H^\pm}$	[80, 1000] GeV
$\sin(\beta-\alpha)$	[0.97, 1]
$\tan\beta$	[0.5, 45]
m_{12}^2	$[0, 10^6]$ GeV^2

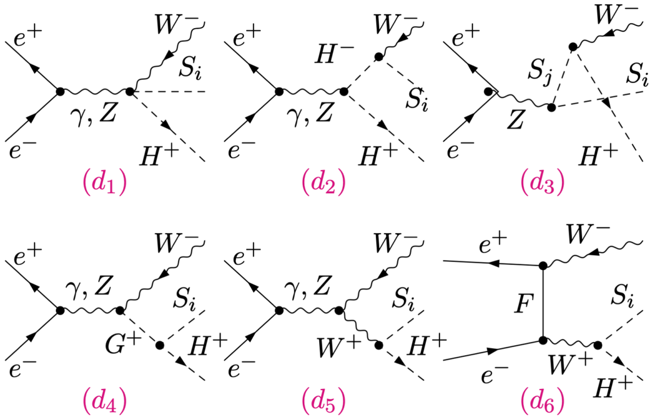

FIG. 1. Tree-level generic Feynman diagrams for $e^+e^- \to H^\pm W^\mp S$ ($S = H$, A) are shown in ($d_{1,\dots,6}$). For all diagrams, S_i refers to H or A. For d_3, if $S_i = H$, S_j should be A, while if $S_i = A$, S_j should be H.

The Yukawa textures only enter in the width of the Higgs propagators. After the Higgses decay into fermions, the result depends on the Yukawa type of the model. Our results here are presented for the type-X 2HDM. It should be noted that the $e^+e^- \to H^\pm W^\mp h$ production process is suppressed by the factor $c^2_{\beta-\alpha}$. To ensure numerical stability of the $2 \to 3$ phase space integration, we introduce the width for the scalar propagators (d_2 and d_3) as well as for the W boson propagators (d_5 and d_6).

In Fig. 2, we show the cross sections for $\sigma(e^+e^- \to H^\pm W^\mp H, H^\pm W^\mp A)$ at $\sqrt{s} = 500$ GeV, 1 TeV, and 1.5 TeV. The process $e^+e^- \to H^\pm W^\mp H$, shown in the top right panel, is controlled by the vertex $H^\pm W^\mp H$, which is proportional to $s_{\beta-\alpha}$ and favored by the alignment, while $e^+e^- \to H^\pm W^\mp A$, illustrated in the top left and bottom panels, is controlled by the $H^\pm H^\mp A$ vertex,

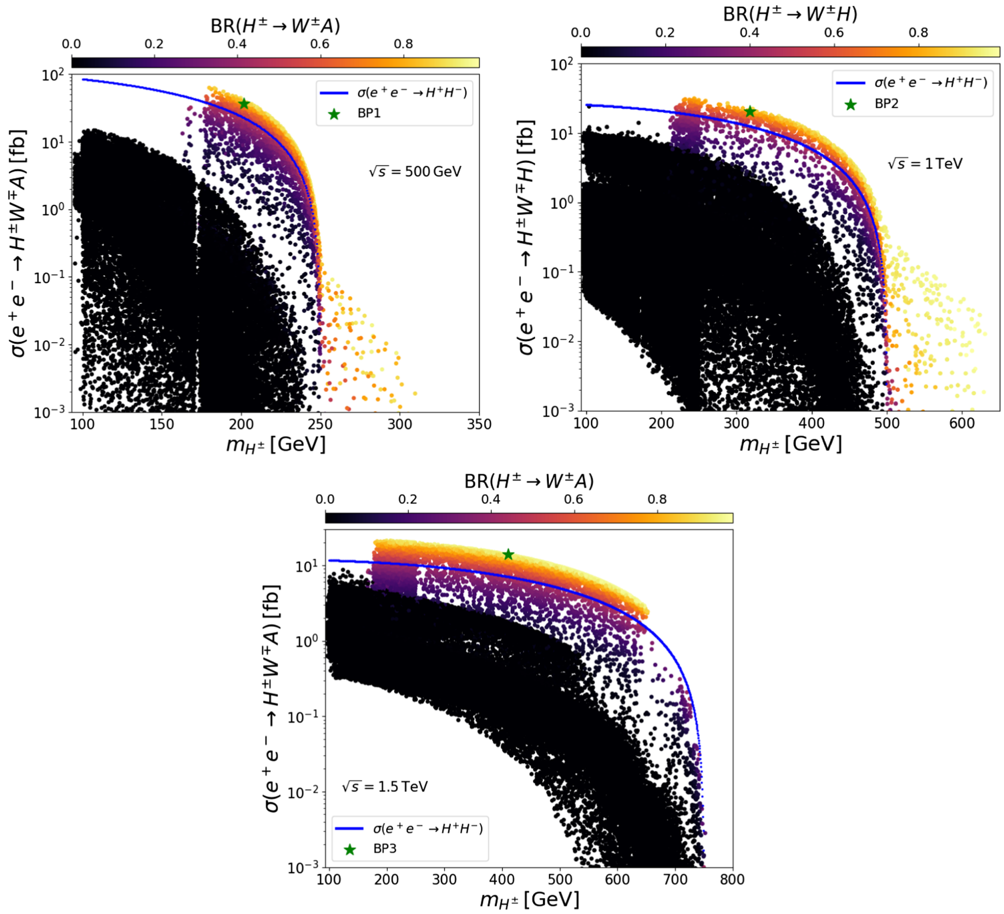

FIG. 2. The cross sections $\sigma(e^+e^- \to H^\pm W^\mp S)$, at different collision energies of the ILC, as a function of $m_{H^\pm}$, with the blue contour lines representing $\sigma(e^+e^- \to H^+H^-)$. The color bar indicates $\mathrm{BR}(H^\pm \to W^\pm S)$. The selected benchmark points (BPs) are highlighted by green stars.

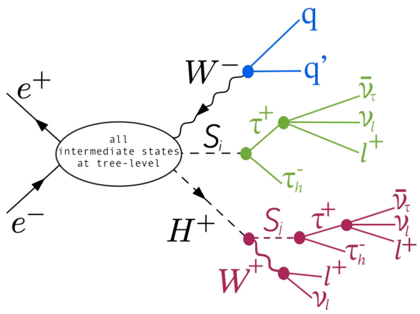

FIG. 3. Diagram illustrating our two signals. Note that our analysis considers all diagrams illustrated in Fig. 1 for $e^+e^- \to H^\pm W^\mp S(S_i = H, A)$ production.

which is independent of the $\beta - \alpha$ mixing. Only Feynman diagram d_3 would have $s_{\beta-\alpha}$ factor coming from $e^+e^- \to AH^* \to H^\pm W^\mp A$. At $\sqrt{s} = 500$ GeV, the process $e^+e^- \to H^\pm W^\mp A$ can reach values as high as 60 fb for favorable mass configurations, particularly near the resonance threshold where the decay $H^\pm \to W^\pm A$ becomes kinematically allowed. For the process $e^+e^- \to H^\pm W^\mp H$ at $\sqrt{s} = 1$ TeV, which is proportional to $s^2_{\beta-\alpha}$, the cross section may reach 25 fb before the opening of $H^\pm \to W^\pm H$, and it would drop as the charged Higgs mass increases. Once we cross the $H^\pm \to W^\pm H$ threshold, one can see an enhancement of the cross section compared to the pair production $e^+e^- \to H^\pm H^\mp$ (blue line) coming from the resonant production originating from $e^+e^- \to H^\pm H^\mp \to H^\pm W^\mp H$: $\sigma(e^+e^- \to H^\pm W^\mp H) = \sigma(e^+e^- \to H^\pm H^\mp) \times \mathrm{BR}(H^\mp \to W^\mp H)$ from diagram d_2 as well as from the other Feynman diagrams. At $\sqrt{s} = 1.5$ TeV, we observe a similar pattern to that at 500 GeV. However, the available phase space for charged Higgs pair production is significantly larger.

In Fig. 3, we present the first diagram, d_1, along with the decays chosen for our signals. However, it is important to emphasize that our analysis thoroughly considers all diagrams, including $d_{1,\ldots,6}$, and their respective decay processes.

IV. SIGNAL-TO-BACKGROUND ANALYSIS

In the previous section, we computed the parton-level cross sections for the proposed channels aimed at probing the $H^\pm$ in the type-X model. While these cross sections are not small, the discovery potential depends on how effectively we can distinguish the signal from relevant backgrounds. In this section, we develop search strategies for comprehensive signal-to-background optimization, utilizing advanced tools that incorporate hard-scattering matrix elements, resonance decays, parton showers, hadronization, hadron decays, and a simplified detector response. We conduct detailed studies of the $[\tau\tau][\tau\tau]WW$ signal. For each center-of-mass energy, a specific BP is selected (see Table III). For each BP, either H or A is considered, but not both, as the decays $H^\pm \to W^\pm H$ and $H^\pm \to W^\pm A$ cannot simultaneously occur due to STU constraints. Note that the selected BPs are further checked using the new versions of HiggsBounds and HiggsSignals via HiggsTools [87].

Signal and background events are generated using MadGraph5_aMC_v3.4.1 [88], where we used the TauDecay library [89] to account for the τ decays. The generated events are then passed to Pythia–8.2 [90] for showering and hadronization. Jet clustering is performed using FastJet [91], and fast detector simulations are conducted with Delphes–3.4.5 [92], utilizing the default Delphes_Card_ILD detector card, which implements the anti-k_t algorithm [93] with a cone radius of $R = 0.4$. Finally, both signals and background events are analyzed using MadAnalysis5 [94].

The $[\tau\tau][\tau\tau]WW$ channel targets the $H^\pm W^\mp S$ production, followed by $H^\pm \to W^\pm S$ ($S = A$, H),

$$\begin{aligned} e^+e^- &\to W^\pm H^\mp S \to W^\pm W^\mp SS \\ &\to W_{qq'} W_{l\nu_l} \tau_h^+ \tau_l^- \tau_h^+ \tau_l^- \\ &\to 3l + \tau_h^+ \tau_h^+ + jj + \not{E}_T, \end{aligned} \tag{5}$$

where $l = e$, μ represents the charged lepton and j designates a light jet. The final state includes three charged leptons, two hadronic τ's, two light jets, and missing transverse energy. Probing the charged Higgs boson in this final state is particularly challenging, making $H^\pm$ mass reconstruction impossible. However, the signal significance at the final selection stage is expected to be significant, showing potential for discovery.

The main SM background contributions come from the processes $t\bar{t}$, $t\bar{t}jj$, Zjj, and W^+W^-jj. Backgrounds such as

TABLE III. The description of our BPs. All masses are in GeV.

	Signal	m_H	m_A	$m_{H^\pm}$	$\tan\beta$	$\sin(\beta-\alpha)$	m^2_{12}	$\mathrm{BR}(H^\pm \to W^\pm S)$	$\mathrm{BR}(S \to \tau^+\tau^-)$
BP1	$H^\pm W^\pm A$	139.6	103.3	201.5	9	0.999	2138.14	0.79	1
BP2	$H^\pm W^\mp H$	188.9	259.3	318.1	21.5	0.999	1652.63	0.80	1
BP3	$H^\pm W^\mp A$	417.4	109.1	410.6	14.8	0.991	11717.46	0.96	1

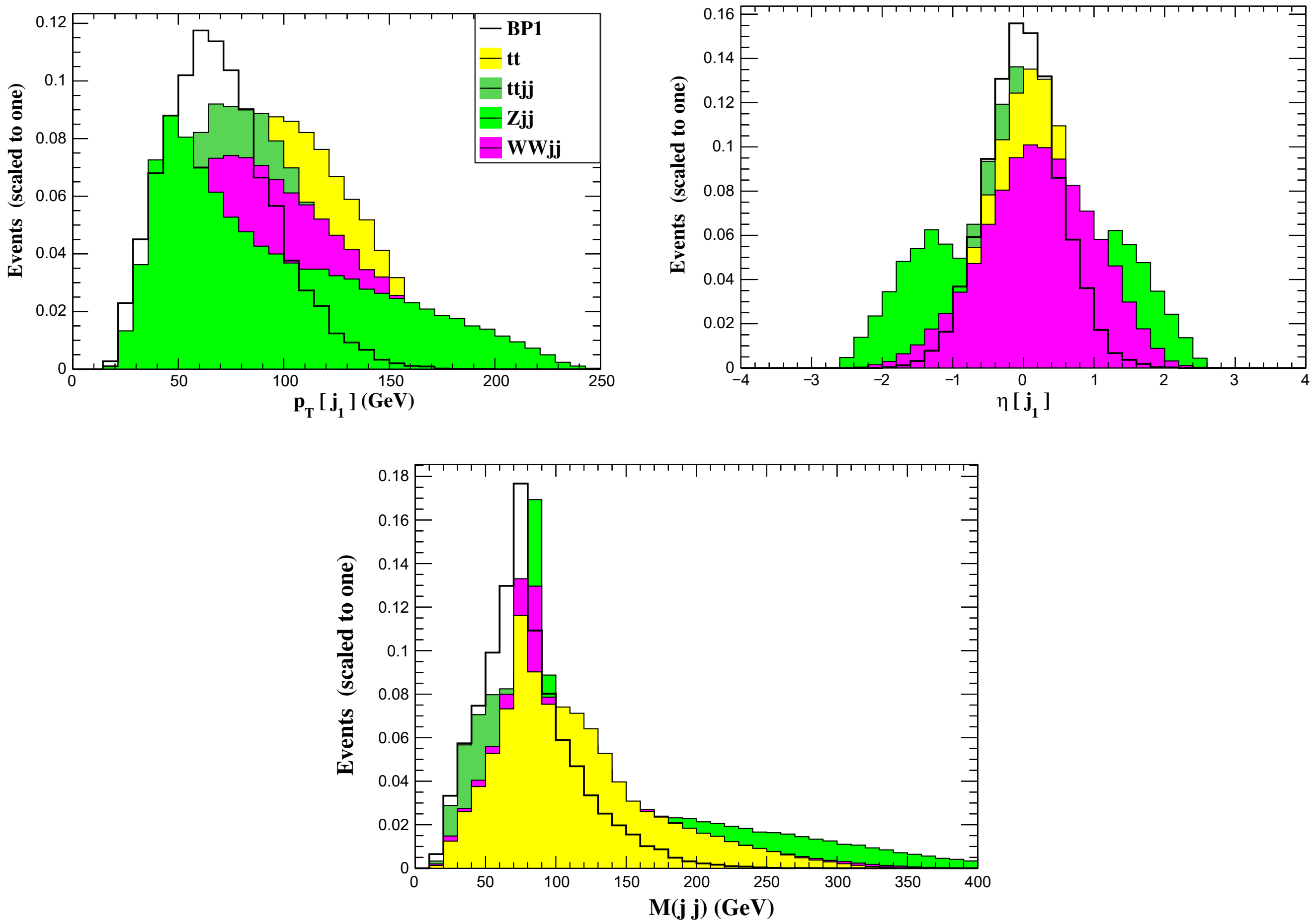

FIG. 4. Selected distributions which we used in the signal to background optimization analysis: the first leading jet transverse momentum $p_T[j_1]$ (top left panel), the pseudorapidity of the first leading jet $\eta[j_1]$ (top right panel), and the mass invariant of the two leading jets $M(jj)$ (lower panel). The backgrounds shown here correspond to $t\bar{t}$ (yellow), $t\bar{t}jj$ (green), Zjj (lime), and $WWjj$ (purple). In this canvas, we show $e^+e^- \to H^\pm W^\mp A$ for BP1.

$t\bar{t}b\bar{b}$, $t\bar{t}X(X = Z, h)$, $t\bar{t}ZZ$, and ZZZ are minor.[2] In each case, one of the top quarks is assumed to decay semileptonically, while the other one decays hadronically. Meanwhile, the boson Z is assumed to decay into a $\tau^+\tau^-$ pair, and one of the W boson is assumed to decay leptonically, while the other one decays into a pair of light jets. The backgrounds are as follows:

(i) $e^+e^- \to t\bar{t}$. $(t \to W^+b, W^+ \to l^+\nu_l)$, $(\bar{t} \to W^-\bar{b}, W^- \to jj)$.
(ii) $e^+e^- \to t\bar{t}jj$, $(t \to W^+b, W^+ \to l^+\nu_l)$, $(\bar{t} \to W^-\bar{b}, W^- \to l^-\nu_l)$.
(iii) $e^+e^- \to Zjj$, $(Z \to \tau^+\tau^-)$.
(iv) $e^+e^- \to W^+W^-jj$, $(W^+ \to jj)$, $(W^- \to l^-\nu_l)$.

For event selection, we take the following steps. The basic cuts consist of

$$p_T^{j,l} \geq 10 \text{ GeV}, \qquad |\eta^{j,l}| < 2.5, \qquad \Delta R^{ll,lj,jj} \geq 0.4. \tag{6}$$

To assess observability, we calculate the significance using the expression

$$\Sigma = \sqrt{\mathcal{L}}\frac{\sigma_s}{\sqrt{\sigma_s + \sigma_b}}, \tag{7}$$

where σ_s and σ_b are both the signal and background cross sections after all the cuts.

A. Process at $\sqrt{s} = 500$ GeV

After applying the cuts on the number of jets and b jets, $N(b) \leq 1$ and $N(l) \geq 3$, which is a key discriminator between the signal and backgrounds. The signal rate remains high, with an acceptance times efficiency $(S \times \epsilon)$ of approximately 42%. In contrast, the total background is reduced to $(B \times \epsilon) = 0.03\%$.

To devise more advanced selection strategies, the kinematic distributions of the signal and backgrounds including the first leading jet transverse momentum[3]

[2]The requirements of three charged leptons and two hadronic taus plus two jets and $N(b) \leq 1$ keep them negligible.

[3]The jets are labeled by descending order of p_T, i.e., $p_T[j_1] > p_T[j_2]$.

TABLE IV. The cut-flow chart of the cross section (in fb) counts for the $[\tau\tau][\tau\tau]WW$ signal and backgrounds, with $\sqrt{s} = 500$ GeV.

Cuts	Signal	Backgrounds			
	BP1	$t\bar{t}$	$t\bar{t}jj$	Zjj	W^+W^-jj
Without cut	0.72	86.2	0.35	15.9	3.2
Basic cut	0.63	74.2	0.29	14.1	2.99
$N(b) \leq 1$ and $N(l) \geq 3$	0.266	0.02	0.004	0.005	0.0003
$P_T[j_1] \leq 80$ and $-0.6 < \eta[j_1] < 0.6$	0.133	0.008	0.0018	0.0004	9.10^{-5}
$M(jj) \leq 130$ GeV	0.1	0.007	0.001	0.0001	9.10^{-5}
Total efficiencies	15.8%	9.10^{-3}	3.10^{-1}	7.10^{-6}	3.10^{-5}

TABLE V. Significance for our signal with $\sqrt{s} = 500$ GeV and $\mathcal{L} = 500$, 1000, and 1500 fb^{-1}.

	BP1		
Processes		$e^+e^- \to H^\pm W^\mp A \to [\tau\tau][\tau\tau]WW$	
Luminosity	$\mathcal{L} = 500$ fb^{-1}	$\mathcal{L} = 1000$ fb^{-1}	$\mathcal{L} = 1500$ fb^{-1}
Significance Σ	6.79	9.61	11.77

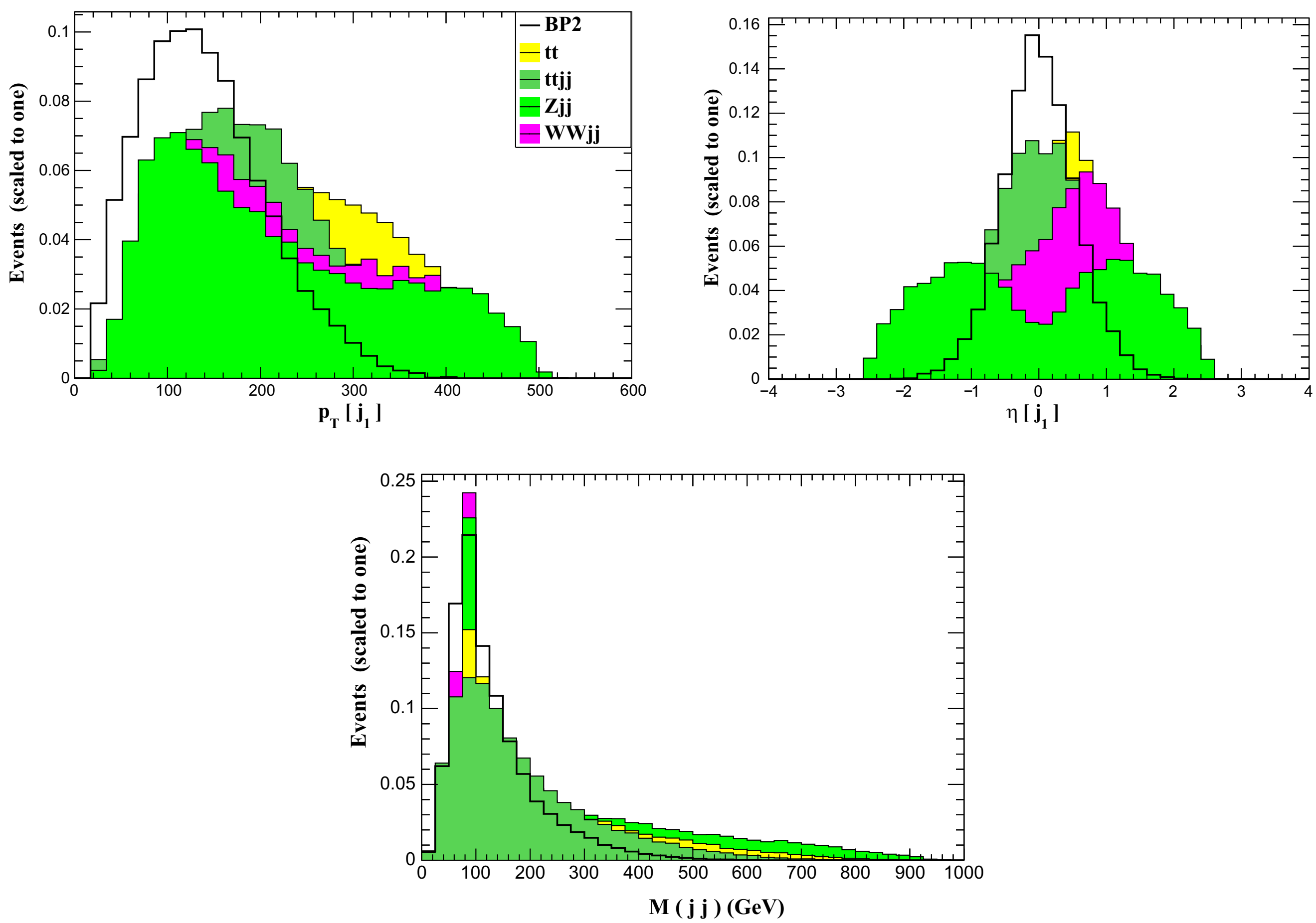

FIG. 5. Selected distributions which we used in the signal to background optimization analysis: the first leading jet transverse momentum $p_T[j_1]$ (top-left panel); the pseudorapidity of the first leading jet $\eta[j_1]$ (top-right panel); and the invariant mass of the two leading jets $M(jj)$ (lower panel). The backgrounds shown here correspond to $t\bar{t}$ (yellow), $t\bar{t}jj$ (green), Zjj (lime), and $WWjj$ (purple). In this canvas, we show $e^+e^- \to H^\pm W^\mp H$ for BP2.

TABLE VI. The cut-flow chart of the cross section (in fb) counts for the $[\tau\tau][\tau\tau]WW$ signal and backgrounds, with $\sqrt{s} = 1$ TeV.

	Signal	Backgrounds			
Cuts	BP2	$t\bar{t}$	$t\bar{t}jj$	Zjj	W^+W^-jj
Without cut	0.41	26.4	1.51	2.78	2.74
Basic cut	0.25	22.5	1.27	2.67	2.71
$N(l) \geq 3$	0.12	0.012	0.021	0.001	0.001
$P_T[j_1] \leq 170$ and $-0.6 < \eta[j_1] < 0.6$	0.079	0.004	0.005	0.0	0.0002
$M(jj) \leq 140$ GeV	0.058	0.002	0.003	0.0	0.0
Total efficiencies	23%	8.10^{-5}	0.23%	⋯	⋯

$p_T[j_1]$ (top-left panel), the pseudorapidity of the first leading jet $\eta[j_1]$ (top-right panel), and the invariant mass of the two leading jets $M(jj)$ (lower panel) are plotted in Fig. 4.

Based on the investigation of the kinematic distributions, we devise a search strategy summarized in Table IV. Consequently, we impose a stringent criterion on the transverse momentum and the pseudorapidity of the leading jet, $P_T[j_1] \leq 80$ and $-0.6 < \eta[j_1] < 0.6$, which significantly reduces a substantial portion of the background. The final selection is the invariant mass of the two leading jets, $M(jj) \leq 130$ GeV, which also removes a large portion of the background events. At the final selection level, 50 signal events and 4 background events survive, assuming $\mathcal{L} = 500$ fb^{-1}.

In Table V, the statistical significance Σ for the signal process $e^+e^- \to H^\pm W^\mp A \to [\tau\tau][\tau\tau]WW$ at $\sqrt{s} = 500$ GeV for three different integrated luminosities: 500, 1000, and 1500 fb^{-1}. As expected, the significance increases with luminosity, with values of 6.79, 9.61, and 11.77, respectively. These results demonstrate the potential observability of the signal across all three considered luminosities of 500, 1000, and 1500 fb^{-1}, making this channel a promising probe for the considered benchmark point.

B. Process at $\sqrt{s} = 1$ TeV

For the signal and background events that pass the basic cuts, we calculate various kinematic distributions. In Fig. 5, we show the distributions of the first leading jet transverse momentum $p_T[j_1]$ (top-left panel), the pseudorapidity of the first leading jet $\eta[j_1]$ (top-right panel), and the invariant mass of the two leading jets $M(jj)$ (lower panel) for the signal benchmark point BP2 and various SM backgrounds at the 1 TeV ILC.

To enhance the signal significance, we implemented a cut-flow strategy guided by the behavior of key kinematic distributions, as summarized in Table VI. We impose cuts, which serve as crucial discriminators distinguishing the signal from the background, on the number of charged leptons: $N(l) \geq 3$. With this cut applied, 48% of the signal events are retained, while the background is significantly suppressed. The first selection cut applied is $P_T[j_1] \leq 170$ GeV and $-0.6 < \eta[j_1] < 0.6$, going together for the detection of the first leading jet. This cut significantly reduces a substantial portion of the background, particularly eliminating the majority of $t\bar{t}$, $WWjj$, and Zjj events. We investigate one of the most effective cuts, $M(jj) \leq 140$ GeV, which keeps approximately 73% of the signal events while eliminating over 54% of the background events. This constitutes the final selection in our cut flow strategy, significantly enhancing the signal-to-background ratio.

In Table VII, the signal significance Σ for the process $e^+e^- \to H^\pm W^\mp H \to [\tau\tau][\tau\tau]WW$ is presented at $\sqrt{s} = 1$ TeV for three integrated luminosities: 500, 1000, and 1500 fb^{-1}. The corresponding significance values are 5.12, 7.25, and 8.87, respectively. This progression demonstrates the enhanced visibility of the signal with increasing luminosity and supports the viability of this channel in probing the BP2 scenario.

C. Process at $\sqrt{s} = 1.5$ TeV

We show in Fig. 6 the kinematic distributions of the signal and the backgrounds at $\sqrt{s} = 1.5$ TeV, specifically the missing transverse energy $\not{E}_T$ (top-left panel), the pseudorapidity $\eta[j_1]$ (top-right panel) of the first leading jet, and the scalar sum of jet missing transverse momentum

TABLE VII. Significance for our signal with $\sqrt{s} = 1$ TeV and $\mathcal{L} = 500$, 1000 and 1500 fb^{-1}.

	BP2		
Process		$e^+e^- \to H^\pm W^\mp H \to [\tau\tau][\tau\tau]WW$	
Luminosity	$\mathcal{L} = 500$ fb^{-1}	$\mathcal{L} = 1000$ fb^{-1}	$\mathcal{L} = 1500$ fb^{-1}
Significant Σ	5.12	7.25	8.87

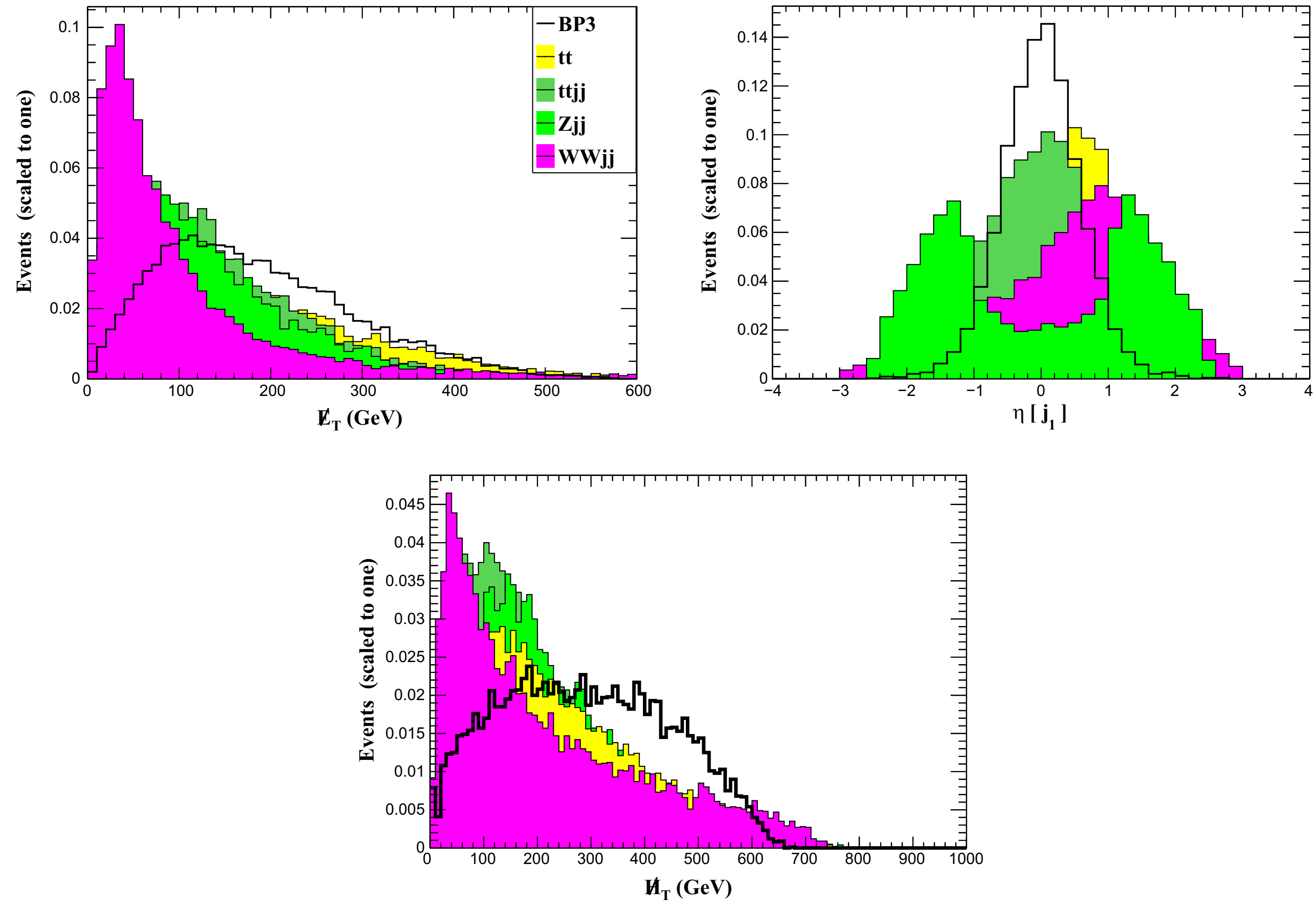

FIG. 6. Selected distributions which we used in the signal-to-background optimization analysis: the missing transverse energy $\not{E}_T$ (top-left panel); the pseudorapidity of the first leading jet $\eta[j_1]$ (top-right panel); and the scalar sum of jet missing transverse momentum $\not{H}_T$ (lower panel). The backgrounds shown here correspond to $t\bar{t}$ (yellow), $t\bar{t}jj$ (green), Zjj (lime), and $WWjj$ (purple). In this canvas, we show $e^+e^- \to H^\pm W^\mp A$ for BP3.

$\not{H}_T$ (lower panel), which includes only the missing energy from the jet activity.

To enhance the signal significance, we implemented a series of selection cuts guided by the behavior of the kinematic distributions. We impose restrictions on the number of b jets and charged leptons, requiring $N(b) \leq 1$ and $N(l) \geq 3$, which serves as a crucial selection to distinguish the signal from background processes. The first selection cut applied is the missing transverse energy requirement $130 < \not{E}_T < 500$ GeV, which removes about 34% of the $t\bar{t}$, 86% of the Zjj, and 100% of $WWjj$ events, while the survival rate for the signal is more than 66%. The cut of $-0.6 < \eta[j_1] < 0.6$ has a certain advantage in separating the signal from the backgrounds, especially Zjj. The final selection is on the scalar sum of jet missing transverse momentum. The selection cut $\not{H}_T > 290$ GeV removes almost all the background events. Table VIII shows the cut flows on the cross sections (in fb) for both the signal and the SM backgrounds at $\sqrt{s} = 1.5$ TeV. Table IX presents the signal significance Σ for the process $e^+e^- \to H^\pm W^\mp A \to [\tau\tau][\tau\tau]WW$ at $\sqrt{s} = 1.5$ TeV, evaluated for integrated luminosities of 500, 1000, and 1500 fb^{-1}. The significance values obtained are 3.8, 5.38, and 6.59, respectively. These results indicate a clear improvement in signal observability with increasing luminosity, confirming the sensitivity of this final state to the BP3 scenario.

TABLE VIII. The cut-flow chart of the cross section (in fb) counts for the $[\tau\tau][\tau\tau]WW$ signal and backgrounds, with $\sqrt{s} = 1.5$ TeV.

	Signal	Backgrounds			
Cuts	BP3	$t\bar{t}$	$t\bar{t}jj$	Zjj	W^+W^-jj
Without cut	0.34	7.1	0.94	0.98	4.48
Basic cut	0.22	6.9	0.9	0.91	3.29
$N(b) \leq 1$ and $N(l) \geq 3$	0.12	0.003	0.01	0.0007	0.0003
$130 < \not{E}_T < 500$ GeV	0.08	0.002	0.004	0.0001	0
$-0.6 < \eta[j_1] < 0.6$	0.06	0.05	0.002	0	0
$\not{H}_T > 290$ GeV	0.03	0	0.001	0	0
Total efficiencies	13.6%	⋯	0.1%	⋯	⋯

TABLE IX. Significance for our signal with $\sqrt{s} = 1.5$ TeV and $\mathcal{L} = 500$, 1000, and 1500 fb^{-1}.

	BP3		
Processes		$e^+e^- \to H^\pm W^\mp A \to [\tau\tau][\tau\tau]WW$	
Luminosity	$\mathcal{L} = 500$ fb^{-1}	$\mathcal{L} = 1000$ fb^{-1}	$\mathcal{L} = 1500$ fb^{-1}
Significante Σ	3.8	5.38	6.59

V. CONCLUSIONS

Within the framework of the type-X 2HDM, we have conducted a comprehensive study of the phenomenology to establish a detailed roadmap for the charged Higgs boson search. In contrast to type II and type Y, where the $b \to s\gamma$ constraint imposes a stringent lower bound on the charged Higgs mass ($m_{H^\pm} \gtrsim 800$ GeV [95]), type I and type X allow for a lighter charged Higgs. However, even in type X, the parameter space is strongly constrained by other experimental constraints, such as those from direct searches for additional Higgs bosons at LEP, Tevatron, and the LHC.

We have examined the single production of $H^\pm$ in association with a W boson and a non-SM Higgs boson H or A at the e^+e^- collider. We showed that the cross section for $e^+e^- \to H^\pm W^\mp H$ and $e^+e^- \to H^\pm W^\mp A$ are promising, where the former could be useful to measure the Higgs mixing parameter $s_{\beta-\alpha}$. Based on these characteristics, we analyzed the $[\tau\tau][\tau\tau]WW$ final state as a probe of charged Higgs bosons at the ILC, finding it to yield a high detection significance.

In this study, we focused on the type-X 2HDM, as the decays $H/A \to \tau^+\tau^-$ are small in the type-I scenario. In contrast, $H/A \to b\bar{b}$ can be large in type I, leading to the $[bb][bb]WW$ final state. A detailed study of such a final state is left for future work.

ACKNOWLEDGMENTS

K. C. is supported in part by the National Science and Technology Council (NSTC) of Taiwan under Grant No. MoST 113-2112-M-007-041-MY3. M. K. is supported by NSTC of Taiwan under the Grant No. 113-2639-M-002-006-ASP. A. A. would like to thank the Department of Physics and CTC, National Tsing Hua University, for their hospitality during the course of this work.

DATA AVAILABILITY

The data are not publicly available. The data are available from the authors upon reasonable request.

[1] G. Aad *et al.* (ATLAS Collaboration), Observation of a new particle in the search for the standard model Higgs boson with the ATLAS detector at the LHC, Phys. Lett. B **716**, 1 (2012).

[2] S. Chatrchyan *et al.* (CMS Collaboration), Observation of a new boson at a mass of 125 GeV with the CMS experiment at the LHC, Phys. Lett. B **716**, 30 (2012).

[3] B. Ait-Ouazghour and M. Chabab, The Higgs potential in 2HDM extended with a real triplet scalar: A roadmap, Int. J. Mod. Phys. A **36**, 2150131 (2021).

[4] B. Grzadkowski, P. Osland, and J. Wudka, Pragmatic extensions of the standard model, Acta Phys. Pol. B **42**, 2245 (2011).

[5] C. N. Karahan and B. Korutlu, Effects of a real singlet scalar on Veltman condition, Phys. Lett. B **732**, 320 (2014).

[6] N. Darvishi and M. Krawczyk, Implication of quadratic divergences cancellation in the two Higgs doublet model, Nucl. Phys. **B926**, 167 (2018).

[7] B. A. Ouazghour, A. Arhrib, R. Benbrik, M. Chabab, and L. Rahili, Theory and phenomenology of a two-Higgs-doublet type-II seesaw model at the LHC run 2, Phys. Rev. D **100**, 035031 (2019).

[8] F. Kling, S. Su, and W. Su, 2HDM neutral scalars under the LHC, J. High Energy Phys. 06 (2020) 163.

[9] F. An *et al.*, Precision Higgs physics at the CEPC, Chin. Phys. C **43**, 043002 (2019).

[10] E. Accomando *et al.* (CLIC Physics Working Group Collaboration), Physics at the CLIC multi-TeV linear collider, in *11th International Conference on Hadron Spectroscopy*, CERN Yellow Reports: Monographs (2004), p. 6, arXiv:hep-ph/0412251.

[11] A multi-TeV linear collider based on CLIC Technology: CLIC conceptual design report, No. CERN-2012-007, SLAC-R-985, KEK-Report-2012-1, PSI-12-01, JAI-2012-001, 2012.

[12] A. Abada *et al.* (FCC Collaboration), FCC-ee: The Lepton Collider: Future circular collider conceptual design report volume 2, Eur. Phys. J. Special Topics **228**, 261 (2019).

[13] M. Bicer *et al.* (TLEP Design Study Working Group Collaboration), First look at the physics case of TLEP, J. High Energy Phys. 01 (2014) 164.

[14] K. Fujii *et al.* (LCC Physics Working Group Collaboration), Tests of the standard model at the international linear collider, arXiv:1908.11299.

[15] A. Arbey *et al.*, Physics at the $e+e-$ linear collider, Eur. Phys. J. C **75**, 371 (2015).
[16] T. Han, D. Liu, I. Low, and X. Wang, Electroweak couplings of the Higgs boson at a multi-TeV muon collider, Phys. Rev. D **103**, 013002 (2021).
[17] T. Han, Z. Liu, L.-T. Wang, and X. Wang, WIMPs at high energy muon colliders, Phys. Rev. D **103**, 075004 (2021).
[18] M. Belfkir, A. Jueid, and S. Nasri, Boosting dark matter searches at muon colliders with machine learning: The mono-Higgs channel as a case study, Prog. Theor. Exp. Phys. **2023**, 123B03 (2023).
[19] A. Jueid, T. A. Chowdhury, S. Nasri, and S. Saad, Probing Zee-Babu states at muon colliders, Phys. Rev. D **109**, 075011 (2024).
[20] S. Jana and S. Klett, Muonic force and neutrino non-standard interactions at muon colliders, Phys. Rev. D **110**, 095011 (2024).
[21] A. Costantini, F. De Lillo, F. Maltoni, L. Mantani, O. Mattelaer, R. Ruiz, and X. Zhao, Vector boson fusion at multi-TeV muon colliders, J. High Energy Phys. 09 (2020) 080.
[22] P. Bandyopadhyay, S. Parashar, C. Sen, and J. Song, Probing Inert Triplet Model at a multi-TeV muon collider via vector boson fusion with forward muon tagging, J. High Energy Phys. 07 (2024) 253.
[23] T. Han, S. Li, S. Su, W. Su, and Y. Wu, Heavy Higgs bosons in 2HDM at a muon collider, Phys. Rev. D **104**, 055029 (2021).
[24] A. G. Akeroyd *et al.*, Prospects for charged Higgs searches at the LHC, Eur. Phys. J. C **77**, 276 (2017).
[25] V. D. Barger, R. J. N. Phillips, and D. P. Roy, Heavy charged Higgs signals at the LHC, Phys. Lett. B **324**, 236 (1994).
[26] ILC Collaboration, The International Linear Collider Technical Design Report—Volume 2: Physics, arXiv:1306.6352.
[27] J. A. Aguilar-Saavedra *et al.* (ECFA/DESY LC Physics Working Group Collaboration), TESLA: The Superconducting electron positron linear collider with an integrated x-ray laser laboratory. Technical design report. Part 3. Physics at an $e+e-$ linear collider, arXiv:hep-ph/0106315.
[28] B. A. Ouazghour, A. Arhrib, K. Cheung, E.-s. Ghourmin, and L. Rahili, Associated charged Higgs boson production within the 2HDM: $e-e+$ versus $\mu-\mu+$ colliders, Phys. Rev. D **110**, 095026 (2024).
[29] S. Komamiya, Searching for charged Higgs bosons at O (1/2-teV to 1-teV) e^+e^- colliders, Phys. Rev. D **38**, 2158 (1988).
[30] S. Kanemura, S. Moretti, and K. Odagiri, Single charged Higgs boson production at next generation linear colliders, J. High Energy Phys. 02 (2001) 011.
[31] A. Brignole, J. R. Ellis, . J. F. Gunion, M. Guzzo, F. I. Olness, G. Ridolfi, L. Roszkowski, and F. Zwirner, in *e^+e^- Collisions at 500 GeV: The Physics Potential, Proceedings of the Workshop, Munich, Annecy, Hamburg, Germany, 1991*, edited by P. M. Zerwas (DESY Report No. DESY92-123A, Hamburg, 1992), p. 2.
[32] A. Arhrib, M. Capdequi Peyranere, W. Hollik, and G. Moultaka, Associated H^-W^+ production in high-energy e^+e^- collisions, Nucl. Phys. **B581**, 34 (2000); **B400**, 400 (2004).
[33] S. Kanemura, Possible enhancement of the $e^+e^- \to H^\pm W^\pm$ cross-section in the two Higgs doublet model, Eur. Phys. J. C **17**, 473 (2000).
[34] B. A. Ouazghour, A. Arhrib, K. Cheung, E. Ghourmin, and L. Rahili, Charged Higgs production at the muon collider in the 2HDM, Phys. Rev. D **109**, 115009 (2024).
[35] J. Abdallah *et al.* (DELPHI Collaboration), Search for charged Higgs bosons at LEP in general two Higgs doublet models, Eur. Phys. J. C **34**, 399 (2004).
[36] G. Abbiendi *et al.* (ALEPH, DELPHI, L3, OPAL, LEP Collaborations), Search for charged Higgs bosons: Combined results using LEP data, Eur. Phys. J. C **73**, 2463 (2013).
[37] A. Abulencia *et al.* (CDF Collaboration), Search for charged Higgs bosons from top quark decays in $p\bar{p}$ collisions at $\sqrt{s} = 1.96$-TeV., Phys. Rev. Lett. **96**, 042003 (2006).
[38] V. M. Abazov *et al.* (D0 Collaboration), Search for charged Higgs bosons in decays of top quarks, Phys. Rev. D **80**, 051107 (2009).
[39] G. Aad *et al.* (ATLAS Collaboration), Search for charged Higgs bosons decaying via $H^+ \to \tau\nu$ in top quark pair events using pp collision data at $\sqrt{s} = 7$ TeV with the ATLAS detector, J. High Energy Phys. 06 (2012) 039.
[40] G. Aad *et al.* (ATLAS Collaboration), Search for charged Higgs bosons through the violation of lepton universality in $t\bar{t}$ events using pp collision data at $\sqrt{s} = 7$ TeV with the ATLAS experiment, J. High Energy Phys. 03 (2013) 076.
[41] M. Aaboud *et al.* (ATLAS Collaboration), Search for charged Higgs bosons produced in association with a top quark and decaying via $H^\pm \to \tau\nu$ using pp collision data recorded at $\sqrt{s} = 13$ TeV by the ATLAS detector, Phys. Lett. B **759**, 555 (2016).
[42] G. Aad *et al.* (ATLAS Collaboration), Search for charged Higgs bosons decaying via $H^\pm \to \tau^\pm\nu$ in fully hadronic final states using pp collision data at $\sqrt{s} = 8$ TeV with the ATLAS detector, J. High Energy Phys. 03 (2015) 088.
[43] M. Aaboud *et al.* (ATLAS Collaboration), Search for charged Higgs bosons decaying via $H^\pm \to \tau^\pm\nu_\tau$ in the $\tau +$ jets and $\tau +$ lepton final states with 36 fb^{-1} of pp collision data recorded at $\sqrt{s} = 13$ TeV with the ATLAS experiment, J. High Energy Phys. 09 (2018) 139.
[44] G. Aad *et al.* (ATLAS Collaboration), Search for charged Higgs bosons produced in top-quark decays or in association with top quarks and decaying via H$\pm \to \tau \pm \nu\tau$ in 13 TeV pp collisions with the ATLAS detector, Phys. Rev. D **111**, 072006 (2025).
[45] S. Chatrchyan *et al.* (CMS Collaboration), Search for a light charged Higgs boson in top quark decays in pp collisions at $\sqrt{s} = 7$ TeV, J. High Energy Phys. 07 (2012) 143.
[46] CMS Collaboration, Search for a charged Higgs boson in pp collisions at $\sqrt{s} = 8$ tev, J. High Energy Phys. 11 (2015) 018.
[47] CMS Collaboration, Search for neutral MSSM Higgs bosons decaying to a pair of tau leptons in pp collisions, J. High Energy Phys. 10 (2014) 160.
[48] V. Khachatryan *et al.* (CMS Collaboration), Search for a charged Higgs boson in pp collisions at $\sqrt{s} = 8$ TeV, J. High Energy Phys. 11 (2015) 018.
[49] A. M. Sirunyan *et al.* (CMS Collaboration), Search for charged Higgs bosons in the $H^\pm \to \tau^\pm\nu_\tau$ decay channel in

proton-proton collisions at $\sqrt{s} = 13$ TeV, J. High Energy Phys. 07 (2019) 142.
[50] CMS Collaboration, Search for charged Higgs bosons with the $H^{\pm} \to \tau^{\pm}\nu_{\tau}$ decay channel in proton-proton collisions at $\sqrt{s} = 13$ TeV, Report No. CMS-PAS-HIG-18-014, 2018.
[51] G. Aad *et al.* (ATLAS Collaboration), Search for a light charged Higgs boson in the decay channel $H^{+} \to c\bar{s}$ in $t\bar{t}$ events using pp collisions at $\sqrt{s} = 7$ TeV with the ATLAS detector, Eur. Phys. J. C **73**, 2465 (2013).
[52] V. Khachatryan *et al.* (CMS Collaboration), Search for a light charged Higgs boson decaying to $c\bar{s}$ in pp collisions at $\sqrt{s} = 8$ TeV, J. High Energy Phys. 12 (2015) 178.
[53] A. M. Sirunyan *et al.* (CMS Collaboration), Search for a light charged Higgs boson in the $H^{\pm} \to$ cs channel in proton-proton collisions at $\sqrt{s} = 13$ TeV, Phys. Rev. D **102**, 072001 (2020).
[54] G. Aad *et al.* (ATLAS Collaboration), Search for a light charged Higgs boson in $t \to H^{\pm}b$ decays, with $H^{\pm} \to cs$, in pp collisions at $\sqrt{s} = 13$ TeV with the ATLAS detector, Eur. Phys. J. C **85**, 153 (2025).
[55] G. Aad *et al.* (ATLAS Collaboration), Search for a light charged Higgs boson in $t \to H^{\pm}b$ decays, with $H^{\pm} \to cb$, in the lepton + jets final state in proton-proton collisions at $\sqrt{s} = 13$ TeV with the ATLAS detector, J. High Energy Phys. 09 (2023) 004.
[56] A. Arhrib, M. Krab, and S. Semlali, Accommodating the LHC charged Higgs boson excess at 130 GeV in the general two-Higgs doublet model, J. Phys. G **51**, 115003 (2024).
[57] A. M. Sirunyan *et al.* (CMS Collaboration), Search for a charged Higgs boson decaying to charm and bottom quarks in proton-proton collisions at $\sqrt{s} = 8$ TeV, J. High Energy Phys. 11 (2018) 115.
[58] G. Aad *et al.* (ATLAS Collaboration), Search for charged Higgs bosons in the $H^{\pm} \to tb$ decay channel in pp collisions at $\sqrt{s} = 8$ TeV using the ATLAS detector, J. High Energy Phys. 03 (2016) 127.
[59] M. Aaboud *et al.* (ATLAS Collaboration), Search for charged Higgs bosons decaying into top and bottom quarks at $\sqrt{s} = 13$ TeV with the ATLAS detector, J. High Energy Phys. 11 (2018) 085.
[60] G. Aad *et al.* (ATLAS Collaboration), Search for charged Higgs bosons decaying into a top quark and a bottom quark at $\sqrt{s} = 13$ TeV with the ATLAS detector, J. High Energy Phys. 06 (2021) 145.
[61] A. M. Sirunyan *et al.* (CMS Collaboration), Search for a charged Higgs boson decaying into top and bottom quarks in events with electrons or muons in proton-proton collisions at $\sqrt{s} = 13$ TeV, J. High Energy Phys. 01 (2020) 096.
[62] A. M. Sirunyan *et al.* (CMS Collaboration), Search for charged Higgs bosons decaying into a top and a bottom quark in the all-jet final state of pp collisions at $\sqrt{s} = 13$ TeV, J. High Energy Phys. 07 (2020) 126.
[63] A. Arhrib, R. Benbrik, and S. Moretti, Bosonic decays of charged Higgs bosons in a 2HDM type-I, Eur. Phys. J. C **77**, 621 (2017).
[64] A. Arhrib, R. Benbrik, H. Harouiz, S. Moretti, Y. Wang, and Q.-S. Yan, Implications of a light charged Higgs boson at the LHC run III in the 2HDM, Phys. Rev. D **102**, 115040 (2020).
[65] H. Bahl, T. Stefaniak, and J. Wittbrodt, The forgotten channels: Charged Higgs boson decays to a $W^{\pm}$ and a non-SM-like Higgs boson, J. High Energy Phys. 06 (2021) 183.
[66] A. Arhrib, R. Benbrik, M. Krab, B. Manaut, S. Moretti, Y. Wang, and Q.-S. Yan, New discovery modes for a light charged Higgs boson at the LHC, J. High Energy Phys. 10 (2021) 073.
[67] A. Arhrib, R. Benbrik, M. Krab, B. Manaut, S. Moretti, Y. Wang, and Q.-S. Yan, New Light H± discovery channels at the LHC, Symmetry **13**, 2319 (2021).
[68] T. Mondal and P. Sanyal, Same sign trilepton as signature of charged Higgs in two Higgs doublet model, J. High Energy Phys. 05 (2022) 040.
[69] A. Arhrib, R. Benbrik, M. Krab, B. Manaut, S. Moretti, Y. Wang, and Q. S. Yan, Light charged Higgs boson in $H^{\pm}h$ associated production at the LHC, in *1st Pan-African Astro-Particle and Collider Physics Workshop* (2022), p. 5, arXiv:2205.14274.
[70] M. Krab, M. Ouchemhou, A. Arhrib, R. Benbrik, B. Manaut, and Q.-S. Yan, Single charged Higgs boson production at the LHC, Phys. Lett. B **839**, 137705 (2023).
[71] A. M. Sirunyan *et al.* (CMS Collaboration), Search for a light charged Higgs boson decaying to a W boson and a *CP*-odd Higgs boson in final states with $e\mu\mu$ or $\mu\mu\mu$ in proton-proton collisions at $\sqrt{s} = 13$ TeV, Phys. Rev. Lett. **123**, 131802 (2019).
[72] ATLAS Collaboration, Search for $H^{\pm} \to W^{\pm}A \to W^{\pm}\mu\mu$ in $pp \to t\bar{t}$ events using an $e\mu\mu$ signature with the ATLAS detector at $\sqrt{s} = 13$ TeV, Report No. ATLAS-CONF-2021-047, 2021.
[73] A. Tumasyan *et al.* (CMS Collaboration), Search for a charged Higgs boson decaying into a heavy neutral Higgs boson and a W boson in proton-proton collisions at $\sqrt{s} = 13$ TeV, J. High Energy Phys. 09 (2023) 032.
[74] G. Aad *et al.* (ATLAS Collaboration), Search for a heavy charged Higgs boson decaying into a W boson and a Higgs boson in final states with leptons and b-jets in $\sqrt{s} = 13$ TeV pp collisions with the ATLAS detector, J. High Energy Phys. 02 (2025) 143.
[75] J. Li, H. Song, S. Su, and W. Su, Charged Higgs search in 2HDM, J. High Energy Phys. 05 (2025) 063.
[76] M. Hashemi and O. Seify, Observability of 2HDM charged Higgs boson in a misaligned scenario, Phys. Rev. D **112**, 035029 (2025).
[77] G. C. Branco, P. M. Ferreira, L. Lavoura, M. N. Rebelo, M. Sher, and J. P. Silva, Theory and phenomenology of two-Higgs-doublet models, Phys. Rep. **516**, 1 (2012).
[78] E. A. Paschos, Diagonal neutral currents, Phys. Rev. D **15**, 1966 (1977).
[79] S. L. Glashow and S. Weinberg, Natural conservation laws for neutral currents, Phys. Rev. D **15**, 1958 (1977).
[80] D. Eriksson, J. Rathsman, and O. Stal, 2HDMC: Two-Higgs-doublet model calculator physics and manual, Comput. Phys. Commun. **181**, 189 (2010).
[81] P. Bechtle, D. Dercks, S. Heinemeyer, T. Klingl, T. Stefaniak, G. Weiglein, and J. Wittbrodt, HiggsBounds-5: Testing Higgs sectors in the LHC 13 TeV era, Eur. Phys. J. C **80**, 1211 (2020).

[82] P. Bechtle, S. Heinemeyer, T. Klingl, T. Stefaniak, G. Weiglein, and J. Wittbrodt, HiggsSignals-2: Probing new physics with precision Higgs measurements in the LHC 13 TeV era, Eur. Phys. J. C **81**, 145 (2021).
[83] F. Mahmoudi, SuperIso v2.3: A program for calculating flavor physics observables in supersymmetry, Comput. Phys. Commun. **180**, 1579 (2009).
[84] T. Hahn and C. Schappacher, The Implementation of the minimal supersymmetric standard model in FeynArts and FormCalc, Comput. Phys. Commun. **143**, 54 (2002).
[85] T. Hahn and M. Perez-Victoria, Automatized one loop calculations in four-dimensions and D-dimensions, Comput. Phys. Commun. **118** (1999) 153,
[86] J. Kublbeck, M. Bohm, and A. Denner, Feyn Arts: Computer algebraic generation of Feynman graphs and amplitudes, Comput. Phys. Commun. **60**, 165 (1990).
[87] H. Bahl, T. Biekötter, S. Heinemeyer, C. Li, S. Paasch, G. Weiglein, and J. Wittbrodt, HiggsTools: BSM scalar phenomenology with new versions of HiggsBounds and HiggsSignals, Comput. Phys. Commun. **291** (2023) 108803,
[88] J. Alwall, R. Frederix, S. Frixione, V. Hirschi, F. Maltoni, O. Mattelaer, H. S. Shao, T. Stelzer, P. Torrielli, and M. Zaro, The automated computation of tree-level and next-to-leading order differential cross sections, and their matching to parton shower simulations, J. High Energy Phys. 07 (2014) 079.
[89] K. Hagiwara, T. Li, K. Mawatari, and J. Nakamura, TauDecay: A library to simulate polarized tau decays via FeynRules and MadGraph5, Eur. Phys. J. C **73**, 2489 (2013).
[90] T. Sjostrand, S. Mrenna, and P. Z. Skands, A brief introduction to Pythia8.1, Comput. Phys. Commun. **178**, 852 (2008).
[91] M. Cacciari, G. P. Salam, and G. Soyez, FastJet user manual, Eur. Phys. J. C **72**, 1896 (2012).
[92] J. de Favereau, C. Delaere, P. Demin, A. Giammanco, V. Lemaître, A. Mertens, and M. Selvaggi (DELPHES 3 Collaboration), Delphes 3, A modular framework for fast simulation of a generic collider experiment, J. High Energy Phys. 02 (2014) 057.
[93] M. Cacciari, G.P. Salam, and G. Soyez, The anti-k_t jet clustering algorithm, J. High Energy Phys. 04 (2008) 063.
[94] E. Conte and B. Fuks, MadAnalysis 5: Status and new developments, J. Phys. Conf. Ser. **523**, 012032 (2014).
[95] M. Misiak, A. Rehman, and M. Steinhauser, Towards $\bar{B} \to X_s\gamma$ at the NNLO in QCD without interpolation in m$_c$, J. High Energy Phys. 06 (2020) 175.